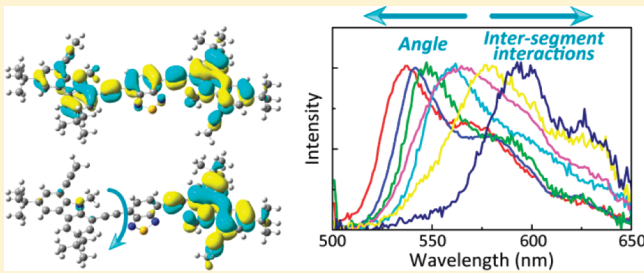


Twist Angle Plays an Important Role in Photophysical Properties of a Donor–Acceptor-Type Conjugated Polymer: A Combined Ensemble and Single-Molecule Study

Satoshi Habuchi,^{*†} Hiroyuki Fujita,[†] Tsuyoshi Michinobu,[‡] and Martin Vacha[†][†]Department of Organic and Polymeric Materials, Tokyo Institute of Technology, Ookayama, Meguro-ku, Tokyo 152-8552, Japan[‡]Global Edge Institute, Tokyo Institute of Technology, Ookayama, Meguro-ku, Tokyo 152-8550, Japan

Supporting Information

ABSTRACT: We investigated photophysical properties of a donor–acceptor-type conjugated polymer by means of ensemble and single-molecule spectroscopy as well as density functional theory (DFT) calculation. The polymer is based on an alkyne-linked 1,8-carbazole (Cz) and possesses a benzothiadiazole (BT) as an electron acceptor moiety. A comparison with model compounds demonstrated that the dimer structure is the spectroscopic unit of the polymer. Single-molecule two-color excitation fluorescence and fluorescence lifetime experiments showed that the polymer molecules displayed broad distributions of fluorescence intensity ratio and fluorescence lifetime. Together with the DFT calculation, we demonstrated that the twist angle between the Cz and BT moieties played a central role in deciding those spectroscopic properties of the polymer. This result was further supported by single-molecule fluorescence spectral measurement. The spectral measurement also suggested intersegment interactions within the single chains. Furthermore, single-molecule defocused and polarization fluorescence imaging suggested efficient exciton migration and trapping occurring within the single polymer chain. These experiments also revealed changes of the lowest energy site within the single polymer molecules.



INTRODUCTION

Conjugated polymers are an important class of materials for optoelectronic applications, such as polymer light-emitting diodes (PLEDs), polymer photovoltaic cells, and field effect transistors.^{1–3} The ease of polymer processing offers potential for enormous cost-savings in those applications. In addition, highly sensitive conjugated polymer-based chemical/biological sensors as well as conjugated polymer dots for biological imaging have also been proposed.^{4–6} Conjugated polymers with electron donor (D)–acceptor (A) architectures have received growing attention.^{7,8} Intramolecular charge transfer (CT) between the D and A moieties in D–A copolymers, allows manipulating their band gaps by carefully selecting the D and A. Due to their small band gaps and broad absorption bands, D–A-type conjugated polymers are of special interest for photovoltaic and white light-emitting applications.^{9,10} For all the device applications, it is of crucial importance to understand photophysical dynamics occurring within individual conjugated polymer chains.

In general, a single conjugated polymer can be described structurally as a large number of quasi-independent conjugated segments over which electron–hole pairs can migrate.¹¹ Each conjugated segment consists of a few to tens of monomer units, depending on the nature of the monomers and microscopic environment surrounding the polymer chain.^{12–16} Intersegment exciton migration (Förster-type energy transfer¹⁷) funnels the

excitation to the lowest-energy segments,^{18,19} resulting in emission from only very localized regions along the chain.^{20,21} This model has been directly demonstrated by single-molecule studies, and is believed to be applicable to a wide range of conjugated polymers.^{19,22–25} The exciton migration processes in conjugated polymers have been studied extensively because these are the decisive factors for the performance of conjugated polymer based devices/materials.^{26,27} For OLED applications, exciton migration to nonemissive sites should be suppressed to extract more light out of the device. On the other hand, efficient exciton migration and eventual quenching are desired for sensor applications. Likewise, the exciton migration to dissociation centers is required for highly efficient photovoltaic cells. Single-molecule studies point to the crucial role of the polymer chain conformation in the exciton migration processes.^{20,28–32} Recent development in optical microscopy techniques actually allows visualization of a nanoscale chain conformation,³³ and allows one to make a direct connection between a polymer chain conformation and nanometer-scale exciton dynamics.^{34–36}

In addition to the intersegment interactions, recent studies suggested that the conformational structure within a segment is

Received: September 29, 2011

Revised: October 31, 2011

Published: November 01, 2011

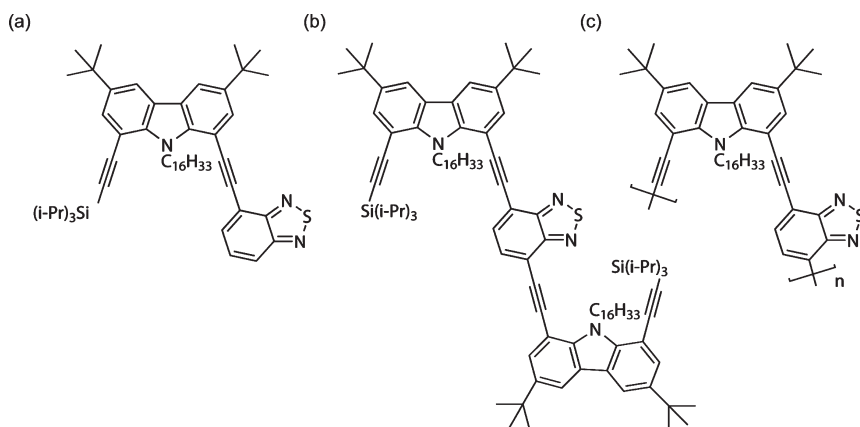


Figure 1. Chemical structure of (a) CzBT, (b) $(\text{CzBT})_2$, and (c) $(\text{CzBT})_n$.

also one of the determining factors of the spectroscopic natures of the conjugated polymer molecules.^{37,38} A single-molecule study on oligo(phenylene-vinylene) derivatives indicated that bending structures within a single segment dominate the spectroscopic properties, i.e., emission energy and spectral width.³⁹ Considering the fact that the CT characteristics of D–A complexes, such as absorption and emission spectra and excited-state lifetime, are often highly related to its structural configuration,⁴⁰ intrasegment configuration would play an especially important role in D–A-type conjugated polymers. In spite of the situation, little attention has been given so far to the intrasegment molecular structures and their impact on the overall photophysical properties of D–A-type conjugated polymers. This is mainly due to the complexities of the excited-state dynamics of this class of polymers⁴¹ to which both intersegment interactions and intrasegment structural configurations have substantial contribution, even at the single-molecule level. Effects of local nanoenvironment surrounding the molecules further complicate excited-state dynamics of D–A-type molecules.^{42,43}

In this study, we investigate the photophysical properties of D–A-type polycarbazole derivatives.⁴⁴ Among a wide range of conjugated polymers, poly(carbazole) derivatives have several unique features such as excellent hole transport properties and good photochemical and environmental stabilities as compared with poly(fluorene) derivatives. These properties make poly(carbazole) derivatives promising materials for optoelectronic applications.^{45–47} Recently, 1,8-carbazole (Cz)-based conjugated polymers emerged as a new class of poly(carbazole) derivatives with the combined physical properties of both 3,6-carbazole and 2,7-carbazole-based derivatives.⁴⁸ Using a variety of single-molecule spectroscopic techniques, we characterize the photophysical properties of a poly(1,8-carbazole)–benzothiadiazole copolymer molecule ($(\text{CzBT})_n$) (Figure 1).^{49,50} We find that the $(\text{CzBT})_n$ molecules show broad distribution of fluorescence peaks and lifetimes. Together with spectroscopic properties of the monomer (CzBT) and dimer ($(\text{CzBT})_2$) model compounds of $(\text{CzBT})_n$ as well as density functional theory (DFT) calculations, we demonstrate that the distributions are dictated by intramolecular twist structures rather than the local environment surrounding the molecules. This result is in stark contrast to previous single-molecule studies on D–A type molecules, which have often attributed the distributions to the local environment surrounding the molecule. We further discuss the

conjugation length and intrachain exciton migration within $(\text{CzBT})_n$ in a comprehensive manner.

EXPERIMENTAL METHODS

Synthetic Procedures. Synthetic procedures of CzBT, $(\text{CzBT})_2$, and $(\text{CzBT})_n$ are provided in the Supporting Information. The chemical structures of the compounds are shown in Figure 1. The weight-average molecular weight (M_w) and the number-average molecular weight (M_n) of $(\text{CzBT})_n$, determined by the comparison of a gel permeation chromatography (GPC) curve (eluent: tetrahydrofuran (THF)) with the calibrated standard polystyrenes, are 8800 and 5400, respectively. The M_n value suggests that the average polymer length is approximately eight repeat units.

Ensemble Spectroscopy. Details of the experimental procedures are provided in the Supporting Information. For solution phase measurements, CzBT, $(\text{CzBT})_2$, and $(\text{CzBT})_n$ were dissolved in solvents at the concentration of 10^{-6} M. Film samples were prepared by embedding $(\text{CzBT})_2$ and $(\text{CzBT})_n$ (5×10^{-5} M) in Zeonex matrices. Absorption and fluorescence spectra of CzBT, $(\text{CzBT})_2$, and $(\text{CzBT})_n$ were recorded using a spectrophotometer (JASCO, V-630) and a spectrofluorometer (JASCO, FP-6200), respectively.

Time-resolved fluorescence measurements were performed using a time-correlated single photon counting method.^{51,52} The excitation light source was a 485 nm pulsed laser (PicoQuant, LDH-P-C-485, pulse width = 100 ps, repetition = 10 MHz). The fluorescence decay curves were analyzed by using the FluoFit software package (PicoQuant).

Single-Molecule Spectroscopy. Detailed procedures of the single-molecule experiments are provided in the Supporting Information (see Figure S1). $(\text{CzBT})_2$ and $(\text{CzBT})_n$ (10^{-10} or 10^{-11} M) were embedded in Zeonex thin films prepared by spin-coating. The samples were vacuum-dried at room temperature for 20 h and used immediately for experiments.

Single-molecule fluorescence images were recorded using an inverted microscope (Olympus, IX71) equipped with a high N.A. objective lens (Olympus, $\times 100$, N.A. = 1.3).^{35,53} A 488 nm line from a CW Ar–Kr ion laser (Coherent, Innova 70) was used for excitation in defocused fluorescence imaging experiments.⁵⁴ The fluorescence signal was collected by the same objective, passed through a dichroic mirror (Omega optical, 500DRLP) and an emission filter (Semrock, BLP01-488R-2S). The fluorescence

images were magnified 3.36 times by using a lens and focused on an electron multiplying charge-coupled device (EM-CCD) camera (Andor technology, iXon^{EM+}, pixel size of the image = 47 nm). Typically, we defocused the images by moving the piezo-electric stage (Nano Control, NS4312-C) toward the objective by an amount of 0.9 μm (Figure S1a). Similar excitation and detection conditions were used for the fluorescence polarization imaging experiments (Figure S1b, excitation power = 34 W cm⁻², illumination area = 45 μm in diameter). Before the images were focused on the EM-CCD camera, they were split into s- and p-polarized images using a polarization beam splitter plate (Edmund Optics, NT47-102). For two-color excitation fluorescence imaging experiments, a 488 and 375 nm CW laser (PicoQuant, LDH-D-C-375) were alternately introduced into the microscope coaxially (Figure S1c).⁵⁵ The fluorescence signal was detected by the EM-CCD camera after passing through the dichroic mirror (Omega optical, 500DRLP) and the emission filter (Semrock, BLP01-488R-25). Single-molecule fluorescence spectra excited at 488 nm were measured by inserting a spectrograph (Bunkoukeiki, CLP-50LD) between the microscope and the CCD camera (Figure S1d).

The single-molecule fluorescence lifetimes of (CzBT)₂ and (CzBT)_n were measured using a homemade stage-scanning confocal fluorescence microscope setup (Figure S1f).^{56,57} A collimated light from the pulsed 485 nm laser was introduced into the microscope objective (Olympus, $\times 100$, N.A. = 1.3). Confocal fluorescence images were recorded by scanning a sample stage using the MFP-3D system of Asylum Research. The fluorescence signal passed through a confocal pinhole and an emission filter, and was detected by an avalanche photodiode (APD). The signal from the APD was split and input into the ARC2 SPM controller system of Asylum Research for imaging and the time-correlated single photon counting PCI-board for fluorescence lifetime measurements. The fluorescence lifetime was measured using a time-tagged time-resolved (TTTR) mode, which allowed reconstructing an intensity trajectory and detected change in the fluorescence lifetime over time.⁵⁶ The TTTR data were analyzed by using the SymPho Time software package (PicoQuant).

DFT Calculation. All quantum mechanical calculations were carried out with the Gaussian09 software package.⁵⁸ Geometry optimizations were performed by using DFT calculations.⁵⁹ In the DFT calculations, the CAM-B3LYP⁶⁰ density functional method was used with the 6-31G(d) basis set. It has been reported that the CAM-B3LYP works better than B3LYP for calculating CT transition.^{61,62} Excitation energy and oscillator strength were determined using time-dependent DFT (TD-DFT) calculations⁶³ at the CAM-B3LYP/6-31++G(d) levels of theory. The transition energy and oscillator strength of the model compounds at fixed twist angles between the Cz and BT unit were also calculated using the same levels of theory.

RESULTS AND DISCUSSION

Fundamental Spectroscopic Properties: Ensemble Absorption and Fluorescence Spectra. CzBT (Figure 2a), (CzBT)₂ (Figure 2c), and (CzBT)_n (Figure 2e) in toluene showed absorption spectra peaking at around 440, 500, 490 nm, respectively (see Table 1). These bands are attributed to intramolecular CT absorption between a donor (Cz) and an acceptor (BT) moieties (see below).^{64,65} The oxidation and reduction potentials of the Cz and BT moieties (1.04 and -1.56 V vs

saturated calomel electrode (SCE), respectively)^{66,67} also suggest that the excited-state CT between the two moieties are energetically favorable process. The CT absorption bands displayed slight blue shifts with increasing the polarity of the solvents (Figure S2, Table 1). The absorption bands that appeared in the shorter wavelength (shorter than 400 nm) can be assigned to a mixture of the CT and local electronic transitions within each moiety (see below).^{64,68} The CT absorption bands of (CzBT)₂ and (CzBT)_n shift to longer wavelengths as compared with that of CzBT. The smaller highest occupied molecular orbital to lowest unoccupied molecular orbital (HOMO–LUMO) energy gap of (CzBT)₂ and (CzBT)_n can be interpreted as larger electron delocalization in the electronic ground states as compared with CzBT (see below). By contrast, the CT absorption bands of (CzBT)₂ and (CzBT)_n exhibit similar peak wavelengths, which is indicative of similar conjugation lengths of these molecules despite the large difference in the unit numbers (see below).

Fluorescence spectra of CzBT (Figure 2b), (CzBT)₂ (Figure 2d), and (CzBT)_n (Figure 2f) excited at the CT absorption bands (440 nm for CzBT, 488 nm for (CzBT)₂ and (CzBT)_n) displayed red shifts in polar solvents, which are typical for fluorescence from CT excited states (Table 1). The fluorescence spectra excited at shorter wavelengths (between 330 and 375 nm) are virtually identical to those excited at the CT absorption bands (data not shown). These results suggest that the fluorescence of CzBT, (CzBT)₂, and (CzBT)_n always occurs from the energetically most stable CT excited states. While CzBT showed a large red shift with increasing the polarity of the solvents (4284 cm⁻¹), (CzBT)₂ and (CzBT)_n exhibited relatively smaller shifts (2086 cm⁻¹ and 940 cm⁻¹ for (CzBT)₂ and (CzBT)_n, respectively). These observations indicate larger dipole moment of CzBT in the excited state as compared with (CzBT)₂ and (CzBT)_n.⁶⁹ CzBT and (CzBT)₂ showed near-unity fluorescence quantum yields (Φ_{fl}) in nonpolar solvents (Table 1). In contrast, (CzBT)_n exhibited a smaller Φ_{fl} in nonpolar solvents (0.37–0.39). Φ_{fl} values in the polar solvents are smaller than those in the nonpolar solvents for all the samples.

Conjugation Unit in (CzBT)_n: Ensemble Time-Resolved Fluorescence Spectroscopy. CzBT and (CzBT)₂ showed single-exponential fluorescence decay curves in all the solvents tested (Figure S3, S4). The fluorescence lifetime (τ_{fl}) ranges from 8.2 to 11.7 ns for CzBT, and from 4.8 to 7.5 ns for (CzBT)₂ (Table 1). Radiative (k_{r}) and nonradiative (k_{nr}) transition rate constants were calculated using Φ_{fl} and τ_{fl} , and summarized in Table 1. As is obvious from the near-unity Φ_{fl} , nonradiative processes are negligible in CzBT and (CzBT)₂. The k_{r} values of (CzBT)₂ in the nonpolar solvents ($2.1\text{--}2.0 \times 10^8 \text{ s}^{-1}$) are twice as large as those in CzBT ($1.0\text{--}1.2 \times 10^8 \text{ s}^{-1}$). The unit number dependent k_{r} values can be interpreted by the Strickler–Berg relation that points to the linear relation between k_{r} and oscillator strengths (f). Therefore, the 2-fold increase in the k_{r} value observed for (CzBT)₂ as compared with CzBT corresponds to the 2-fold increase of f in (CzBT)₂ as compared with CzBT (see below). Since f is proportional to the conjugation length,^{70,71} these results suggest electron delocalization over the whole molecule in the ground state of (CzBT)₂. This is in good agreement with the CT transition energy of (CzBT)₂ which is smaller than that of CzBT.

In contrast to CzBT and (CzBT)₂, which show the single-exponential behavior of fluorescence decay, fluorescence decay curves of (CzBT)_n always displayed double-exponential behavior

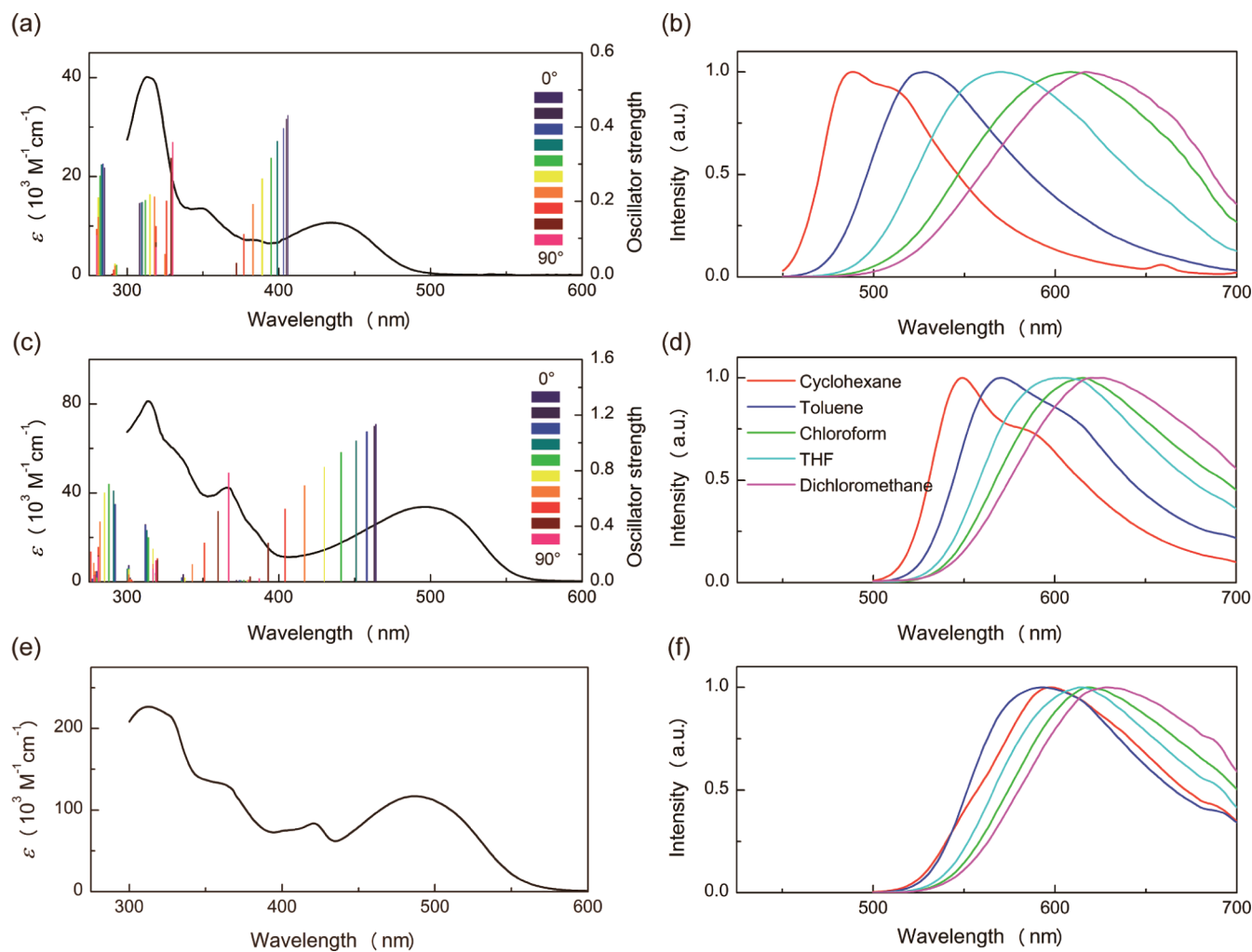


Figure 2. Absorption spectra of (a) CzBT, (c) $(\text{CzBT})_2$, and (e) $(\text{CzBT})_n$ in toluene, respectively. The colored bars represent oscillator strengths of absorption transitions from the ground to excited states in CzBT-M and $(\text{CzBT})_2\text{-M}$ obtained by the DFT calculation, respectively. The oscillator strengths calculated for CzBT-M and $(\text{CzBT})_2\text{-M}$, which have different twist angles of the Cz and BT units, were depicted in different colors. Fluorescence spectra of (b) CzBT, (d) $(\text{CzBT})_2$, and (f) $(\text{CzBT})_n$ in cyclohexane, toluene, chloroform, THF, and dichloromethane, respectively.

Table 1. Solution Phase Ensemble Spectroscopic Parameters of CzBT, $(\text{CzBT})_2$, and $(\text{CzBT})_n$ ^a

sample	solvent	λ_{abs} (nm)	λ_{fl} (nm)	Φ_{fl}	$\tau_{\text{fl}}^{\text{ave}}$ (ns)	k_r (s^{-1})	k_n (s^{-1})
CzBT	cyclohexane	436	488	0.96	8.18	1.2×10^8	4.9×10^6
	toluene	431	529	1.00	9.71	1.0×10^8	N.A.
	chloroform	431	608	0.65	10.3	6.3×10^7	3.4×10^7
	THF	424	570	0.91	11.7	7.7×10^7	8.0×10^6
	dichloromethane	425	617	0.64	11.4	5.6×10^7	3.2×10^7
$(\text{CzBT})_2$	cyclohexane	492	549	0.99	4.82	2.1×10^8	1.1×10^6
	toluene	492	570	0.99	5.05	2.0×10^8	1.2×10^6
	chloroform	490	616	0.95	6.86	1.4×10^8	7.4×10^6
	THF	486	606	0.97	6.59	1.5×10^8	4.1×10^6
	dichloromethane	485	620	0.79	7.47	1.1×10^8	2.8×10^7
$(\text{CzBT})_n$	cyclohexane	500	597	0.37	3.89	7.3×10^7	1.8×10^8
	toluene	487	593	0.39	3.62	1.1×10^8	1.7×10^8
	chloroform	486	619	0.27	3.40	8.0×10^7	2.1×10^8
	THF	482	614	0.25	3.38	7.5×10^7	2.2×10^8
	dichloromethane	484	628	0.18	3.38	5.3×10^7	2.4×10^8

^a λ_{abs} : peak absorption wavelength, λ_{fl} : peak fluorescence wavelength, Φ_{fl} : fluorescence quantum yield, $\tau_{\text{fl}}^{\text{ave}}$: fluorescence lifetime for CzBT and $(\text{CzBT})_2$. Average fluorescence lifetime for $(\text{CzBT})_n$, k_r : radiative rate constant, k_n : non-radiative rate constant.

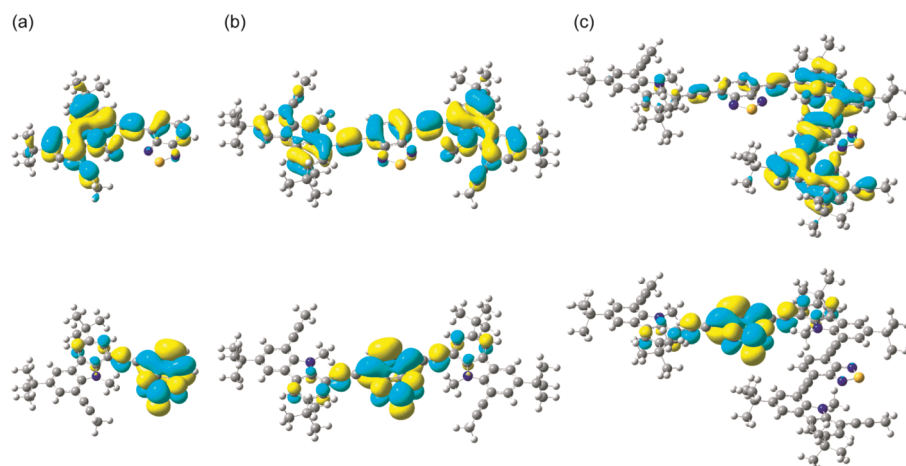


Figure 3. Energetically most stable structures of (a) CzBT, (b) (CzBT)₂, and (c) (CzBT)_n in the ground state. Top and bottom panels show the molecular orbitals of the HOMO and LUMO states, respectively.

(Figure S5, Table S1). The average fluorescence lifetime ($\tau_{\text{fl}}^{\text{ave}}$) of (CzBT)_n was not dependent significantly on the solvents, and had similar values in all the solvents (3.4–3.9 ns, Table 1). While the double-exponential behavior of the fluorescence decays could be attributed to a distribution of the conjugation length in (CzBT)_n, the smaller Φ_{fl} and larger $k_{\text{nr}}^{\text{ave}}$ of (CzBT)_n as compared with those in CzBT and (CzBT)₂ rather indicate the presence of quenching paths of the excited state in (CzBT)_n, which are probably due to interchromophoric interactions within the chain.^{72–74} Both the steady state spectra and the time-resolved fluorescence measurements strongly suggest that the dimer structure is the conjugation unit in (CzBT)_n.

Effect of Chain Structure on Electron Delocalization: DFT Calculation. DFT calculations were performed on CzBT-M, (CzBT)₂-M, and (CzBT)₃-M, which are model compounds of CzBT, (CzBT)₂, and (CzBT)_n, respectively (see Figure S6). In the model compounds, long alkyl chains (C₁₆) on the Cz moiety and Si(i-Pr)₃ groups were replaced by methyl groups. Also (CzBT)_n was modeled by a trimer structure. The calculation shows that CzBT-M takes a coplanar structure of the Cz and BT moiety in a ground state (Figure 3a). (CzBT)₂-M and (CzBT)₃-M also have nearly coplanar structure of the Cz and BT moieties in the ground state. Torsional angles between the two Cz groups in (CzBT)₂-M and (CzBT)₃-M are about 6° and 9°, respectively.

In CzBT-M and (CzBT)₂-M, the electrons delocalize over the Cz and BT moieties in the HOMO energy levels (Figure 3a,b). On the other hand, the electrons are localized on the BT moiety in the LUMO states (Figure 3a,b). These results demonstrate the CT nature of the HOMO–LUMO (S_0 – S_1) transitions observed for CzBT and (CzBT)₂ (Figure 2a,c). Energy gaps and corresponding oscillator strengths (f_{DFT}) for the S_0 – S_1 transition as well as the S_0 – S_n transition in CzBT-M and (CzBT)₂-M obtained by the DFT calculations qualitatively agree with the absorption spectra of CzBT and (CzBT)₂, respectively. f_{DFT} of (CzBT)₂-M is roughly twice as large as that of CzBT. This result perfectly supports the interpretation of the unit number dependent fluorescence lifetime (Table 1). The DFT calculations suggest that the transitions into higher excited states have mixed nature of CT and local transition. In contrast to CzBT-M and (CzBT)₂-M, (CzBT)₃-M does not display electron delocalization all over the molecule in the HOMO energy level (Figure 3c). Instead, the electron delocalizes over the two CzBT units, which

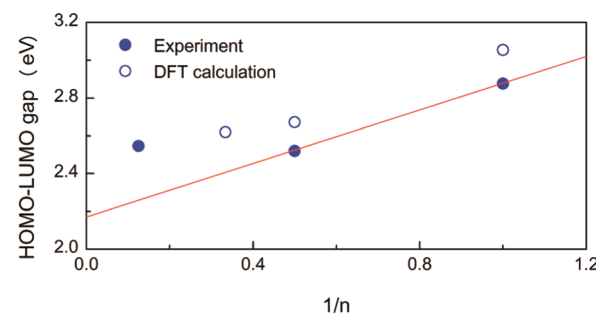


Figure 4. Unit number (n) dependence of the experimentally determined (filled circles) and theoretically calculated (open circles) HOMO–LUMO energy gaps.

is similar to the electron delocalization observed in (CzBT)₂-M. In the LUMO state, the electron localizes on the BT moiety. These results are consistent with the experimental observations that the CT transition energy in (CzBT)₂ and (CzBT)_n are nearly identical (Figure 2c,e).

Figure 4 summarizes the HOMO–LUMO energy gaps determined from the absorption spectra (CT transitions) and the DFT calculations. Both the experimental results and the theoretical calculations demonstrate that the energy gap and the inverse of the unit number (n) have a positive correlation. A linear relationship between $1/n$ and the energy gap is expected for a conjugation system in which a perfect electron delocalization over the entire molecular chain occurs.^{12,13} Deviations from the linear relationship are more evident when n is larger than two, indicating that the electron delocalization over the CzBT polymer chain is limited to the two units. The limited electron delocalization observed for (CzBT)_n in the HOMO level is in contrast to a delocalized HOMO level observed for a related CT-type conjugated polymer, poly(9,9-di-*n*-octylfluorene-*alt*-benzo-thiadiazole) (F8BT), which consists of directly connected fluorene and BT moieties.^{75,76} The difference in electron delocalization could arise from either the acetylene bridge present in (CzBT)_n or the difference in the substitution position.

It has recently become recognized that conjugated polymers can have intrasegment distorted structures.⁷⁷ Especially in D–A type polymers, a torsional angle between D and A has been

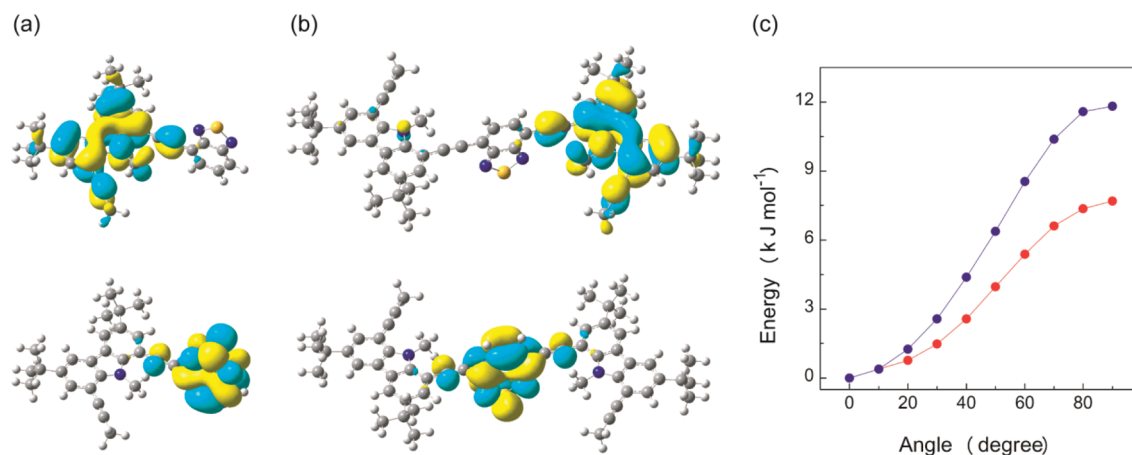


Figure 5. Energetically most stable structures of (a) CzBT-M and (b) (CzBT)₂-M in the ground state with the fixed twist angle between the Cz and BT units at 90°. Top and bottom panels show the molecular orbitals of HOMO and LUMO states, respectively. (c) Twist angle-dependent ground state energy of CzBT-M (red circles) and (CzBT)₂-M (blue circles).

suggested to have a significant effect on their spectroscopic properties,⁷⁸ including exciton migration.³⁷ We performed DFT calculation on CzBT-M and (CzBT)₂-M with fixed angles between the Cz and BT moieties. Figure 5 depicts most stable geometries and molecular orbitals of CzBT-M (Figure 5a) and (CzBT)₂-M (Figure 5b) in the HOMO (top) and LUMO (bottom) energy levels with the twist angle (θ) of 90°. These results demonstrate that electron delocalization across the entire molecule is inhibited by the torsion of the Cz and BT moieties. The electrons are localized on the Cz moiety in the HOMO levels with this geometry. Figure 5c shows HOMO level energy of CzBT-M and (CzBT)₂-M with a range of twist angles ($\theta = 0\text{--}90^\circ$). The HOMO level energies of the twist configuration ($\theta = 90^\circ$) in CzBT-M and (CzBT)₂-M are 8 and 12 kJ/mol higher than those in the most stable coplanar geometries. These results also indicate that the twist configurations (θ up to 40°) can be induced by thermal energy at room temperature. It should be mentioned that the coplanar configuration is not necessarily the most stable geometry in CzBT, (CzBT)₂, and (CzBT)_n. The alkyl chains on the Cz moiety, which are omitted in the DFT calculation, might induce a twist configuration due to steric hindrance. The DFT calculations also suggests that the HOMO–LUMO energy gap increases with increasing twist angle (Figure 2a,b).

Exciton Migration and Trapping: Single-Molecule Defocused and Polarization Fluorescence Imaging. The ensemble spectroscopic measurements and DFT calculations revealed that the CzBT dimer is the spectroscopic (conjugation) unit of (CzBT)_n. Since each (CzBT)_n consists of on average eight CzBT units, (CzBT)_n consists of four spectroscopic units. When there is no spectroscopic interaction between the adjacent units, each unit behaves as an independently emitting chromophore.²⁹ When an efficient intrachain exciton migration occurs, on the other hand, the entire chain behaves like a single chromophore.²⁹ In this case, fluorescence occurs only from a lowest energy unit. We try to characterize the spectroscopic interaction between the units by using single-molecule experiments.

Single-molecule defocused fluorescence imaging allows determining three-dimensional orientation of a single chromophore by analyzing a fluorescence pattern obtained from a single molecule recorded at a slightly defocused condition, thus the method provides an effective tool to investigate physical and optical properties of polymer materials^{54,79–81} Figure 6a shows theoretically

calculated defocused patterns obtained for a molecule whose three-dimensional orientation is defined by angle θ and ϕ . Defocused patterns obtained from individual (CzBT)₂ molecules matched the theoretically calculated patterns, and the patterns underwent very little change over time (Figure 6b, inset). These results indicate the presence of only one emitter within each (CzBT)₂ molecule. This is consistent with the results obtained from the ensemble experiments that suggest that the dimer structure of CzBT is the spectroscopic unit. Fluorescence intensity trajectories of (CzBT)₂ display one step photobleaching, which is also typical for a single chromophoric system (Figure 6b).

By contrast, individual (CzBT)_n molecules displayed stepwise and intermittent fluorescence intensity trajectories (Figure 6c). This type of intensity trajectory is often observed for conjugated polymer molecules that show efficient intramolecular exciton migration.⁸² The efficient exciton migration results in fluorescence emission occurring from a single lowest unit. When this unit is temporally or permanently photooxidized, the entire fluorescence disappears. Therefore, the intermittent trajectory has been connected to the efficient exciton migration.²⁹ The exciton migration occurring within conjugated polymers has been connected mainly to Förster-type energy transfer. Indeed, the Förster-type transfer between CT states and a competitive energy and electron transfer were reported previously.^{83,84} The Förster mechanism is characterized by a Förster radius (R_0), which is the distance between the energy donor and acceptor where the transfer efficiency is 50%. The R_0 of (CzBT)_n in a Zeonex matrix is estimated to be 3.4 nm (Figure S7). Thus, in theory, intramolecular Förster-type exciton migration occurs efficiently in (CzBT)_n. Indeed, the defocused patterns obtained from a molecule depicted in the top panel of Figure 6c support the picture. The defocused patterns obtained from this molecule always match one of the patterns depicted in Figure 6a, which suggest the presence of only one emitting unit within the molecule. 36% (27/75) of the measured molecules fall into this category. Importantly, most of the molecules in this category showed pattern changes over time. This observation suggests that the emitting site in these molecules changes over time. These observations are perfectly consistent with the well-known exciton migration and trapping model proposed for many conjugated polymers.

The bottom panel of Figure 6c shows another type of intensity trajectory and corresponding defocused patterns obtained from a

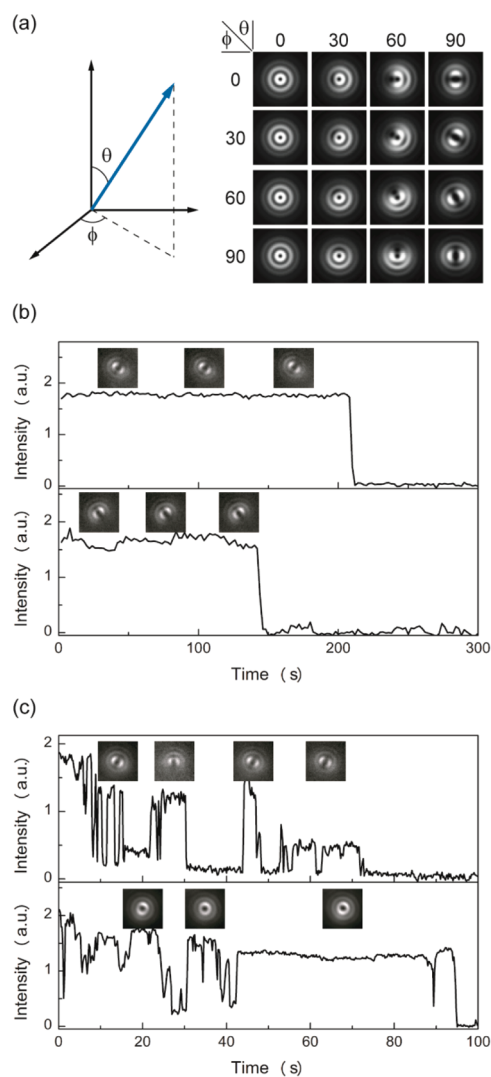


Figure 6. (a) Theoretically calculated defocused fluorescence images of a single molecule whose 3D orientation is defined by θ and ϕ . Examples of fluorescence intensity trajectories (excited at 488 nm) and corresponding defocused fluorescence images obtained from single (b) $(\text{CzBT})_2$ and (c) $(\text{CzBT})_n$ molecules embedded in Zeonex thin films.

single $(\text{CzBT})_n$ molecule. Forty-five percent (34/75) of the measured molecules fall into this category. Those molecules also showed stepwise intermittent trajectories, which point to the efficient exciton migration and trapping taking place within the molecules. However, the defocused patterns cannot be assigned to any three-dimensional orientations in these molecules. Indeed, the patterns are the summation of multiple different patterns,⁸⁵ indicating the presence of simultaneous multiple emitters in the molecule. It should be mentioned that while overlapped defocused patterns can be separated in a well-defined system,⁸⁶ that is not possible in our complex CT polymer. This observation appears to be inconsistent with the intermittent intensity trajectory. A possible explanation for these observations is that the fluorescence occurs from a single unit due to the efficient exciton migration and trapping, but the emitting unit moves rapidly to other units within the exposure time of the imaging acquisition, 200 ms.⁸⁵ In this case, the energy level of each unit would be nearly identical. A slight fluctuation of the energy level

caused by interaction with local environments probably leads to the rapid changes of the emitting units. Switching between the two types was observed for 19% (14/75) of the molecules (Figure S8).

Single-molecule fluorescence polarization measurements (Figure S9) provide further insight into the complicated exciton migration occurring within individual $(\text{CzBT})_n$ molecules. Fluorescence polarization (P) values obtained from individual $(\text{CzBT})_2$ molecules remain constant over time (Figure 7a). A frequency histogram of the P values shows peaks around the minimum and maximum values (Figure 7c). Note that the slight offset for the minimum value is due to the transmission/reflection properties of the polarized beam splitter used in the experiment. The shape of the histogram agrees very well with a calculated histogram for randomly oriented single molecules that consist of only one emitter (Figure S10a). P value trajectories obtained from $(\text{CzBT})_n$ showed more complicated behavior. Jumps in the intensity and P value trajectories are sometimes correlated (Figure 7b top). While the result is in agreement with the exciton migration and trapping model, this result is also compatible with the simultaneous multiple emitter model. Some molecules show sudden jumps of P values without noticeable changes in the intensity (Figure 7b bottom). This result supports the efficient exciton migration and the rapid changes of the emitting units (lowest energy units). Such complicated behavior is summarized in a P value histogram (Figure 7d). The histogram shows a broad distribution with a peak around $P = 0$. The histogram can be well reproduced by a simulated histogram assuming that each molecule contains randomly oriented two or three simultaneously emitting chromophores (Figure S10b,c).^{82,87} This result can be also interpreted by the model based on exciton migration with rapid changes of the emitting units.

Both the defocused imaging and fluorescence polarization experiments support the intramolecular exciton migration occurring within individual $(\text{CzBT})_n$ molecules. However, those experiments also suggest that the kinetics of the changes of the emitting sites varies significantly among individual molecules. Note that a chain length distribution of $(\text{CzBT})_n$ would play a minor role in the exciton migration processes because there is no correlation between the brightness of the emission (i.e., chain length) and the defocused patterns and/or the polarization trajectories.

Structural Distortion in Individual Molecules: Single-Molecule Two-Color Excitation Fluorescence Imaging and Fluorescence Lifetime Experiments. The ensemble experiments demonstrated that $(\text{CzBT})_n$ displayed fluorescence only from the CT state, irrespective of the excitation wavelengths (375 or 488 nm). This was also confirmed at the single-molecule level by illuminating $(\text{CzBT})_n$ molecules with 375 nm light. A fluorescence signal was detected only from the CT state for all the molecules (data not shown).

Figure 8a shows fluorescence intensity trajectories obtained from the CT state of single $(\text{CzBT})_n$ molecules excited at 375 and 488 nm alternatively (see also Figure S11). A perfect correlation between the two trajectories was observed. The ratio between the fluorescence intensity obtained with the 488 and 375 nm excitation ($\text{Int}^{488}/\text{Int}^{375}$) remains constant over time. Single-molecule fluorescence polarization experiments with the 375 and 488 nm excitations also demonstrated that the P value trajectories obtained with the 488 and 375 nm excitation always displayed perfect correlations (Figure S12). These results demonstrate that the photophysical properties of $(\text{CzBT})_n$ are predominantly determined by the nature of the CT state even initially excited into the higher excited states.

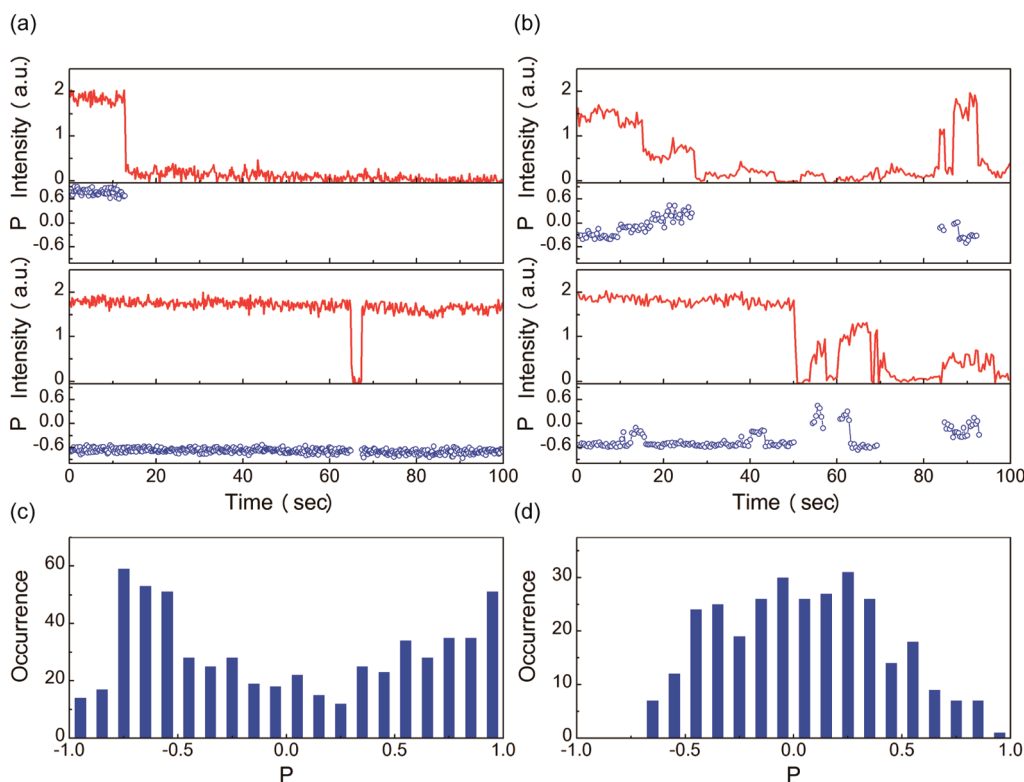


Figure 7. Fluorescence intensity trajectories (top panels) and polarization values (bottom panels) obtained from single (a) $(\text{CzBT})_2$ and (b) $(\text{CzBT})_n$ molecules embedded in Zeonex thin films. Frequency histograms of polarization values obtained for (c) $(\text{CzBT})_2$ and (d) $(\text{CzBT})_n$.

By contrast, each molecule showed a different fluorescence intensity ratio upon excitation at 375 and 488 nm. A frequency histogram of $\text{Int}^{488}/\text{Int}^{375}$ shows broad distribution (Figure 8b). Since the fluorescence always occurs from the same CT state for both 375 and 488 nm excitation, it is unlikely that each molecule has different fluorescence quantum yields for 375 and 488 nm excitations. The finding rather indicates that each molecule has different absorption probabilities for the 375 and 488 nm lights. The different absorption probability could be accounted for by the twist angle-dependent oscillator strength of $(\text{CzBT})_n$. According to the DFT calculation (Figure 2c), the excitation at 488 and 375 nm corresponds to the HOMO–LUMO transition and transition into a higher excited state. As seen in Figure 2c, the oscillator strength of the HOMO–LUMO transition decreases with increasing twist angle (Figure 8c). On the other hand, the oscillator strength of the transition into a higher excited state by 375 nm excitation increases with increasing twist angle (Figure 8c). Therefore, a $(\text{CzBT})_n$ molecule that has a twist structure should exhibit a smaller $\text{Int}^{488}/\text{Int}^{375}$ value as compared with molecules that adopt more coplanar structures. These results suggest that the $(\text{CzBT})_n$ molecules in the Zeonex film adopt different fixed twist angles.

Fluorescence lifetime experiments provide further support for the hypothesis. An ensemble sample of $(\text{CzBT})_2$ in the Zeonex film showed a single exponential decay with fluorescence lifetime of 5.0 ns (Figure S13a). This is in good agreement with the fluorescence lifetime of $(\text{CzBT})_2$ in toluene. At the single-molecule level, $(\text{CzBT})_2$ molecules showed single-exponential decays with an average lifetime of 4.6 ns (Figure 9a).

An ensemble sample of $(\text{CzBT})_n$ in the Zeonex film showed a double-exponential decaying behavior ($\tau_{f1} = 3.4$ ns, $\tau_{f2} = 5.8$ ns), similar to that in a solution (Figure S13b). The average lifetime in

the Zeonex film ($\tau_{av} = 4.4$ ns) is longer than that in the toluene solution. The individual $(\text{CzBT})_n$ molecules showed either single- or double-exponential decays in the initial stage, i.e., before photobleaching (Figure S14). More importantly, initial lifetimes obtained from individual $(\text{CzBT})_n$ molecules ranged between 3.5 and 8 ns with an average value of 5.4 ns (Figure 9b), which is much broader than that of $(\text{CzBT})_2$. A lifetime of 3.5–5 ns agrees well with the lifetime of $(\text{CzBT})_n$ in the toluene solution. On the other hand, a lifetime of 6–8 ns is actually close to that of CzBT. This result suggests that part of the $(\text{CzBT})_n$ molecules in the Zeonex film have an electronic state similar to that of CzBT. The DFT calculations demonstrate that the electron delocalization is inhibited when the Cz and BT moieties are twisted. Together with the single-molecule two-color excitation fluorescence measurements, these findings strongly suggest that each $(\text{CzBT})_n$ molecule has a different Cz–BT angle. Because the thermal energy is estimated to induce the twist of the Cz and BT up to 40° (Figure 5c), additional force is required to further twist the molecule to limit the electron delocalization to one CzBT unit. A force acting on the molecules during the spin coating process might induce the twist conformation.

It should be mentioned that, in the single-molecule lifetime experiments, most of the molecules showed a decrease in fluorescence lifetime after prolonged illumination (Figure S15). This is most probably related to photoinduced generation of an excited-state quencher. The decrease in the fluorescence lifetime upon illumination has also been observed for other conjugated polymers,¹⁹ and has been connected to photoinduced oxidation (hole injection) of the emitters.^{22,88}

Intrasegment Structure and Intersegment Interactions: Single-Molecule Fluorescence Spectra. An ensemble fluorescence

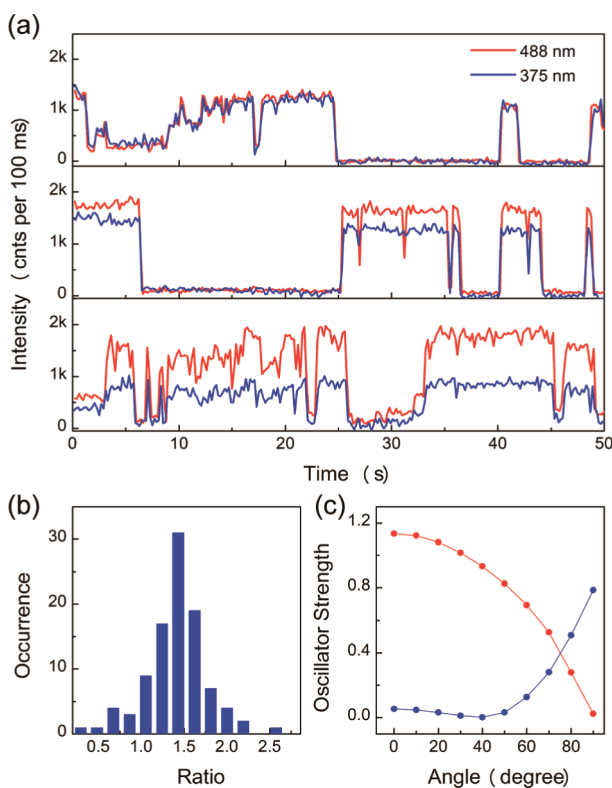


Figure 8. (a) Two-color excitation fluorescence intensity trajectories of single $(\text{CzBT})_n$ molecules embedded in a Zeonex thin film. The red and blue lines show intensity trajectories obtained with the 488 and 375 nm excitation, respectively. (b) Frequency histogram of the ratio of fluorescence intensity obtained by the 488 and 375 nm excitation. (c) Twist angle-dependent oscillator strengths for the HOMO–LUMO (CT) transition (red circles) and transition into a higher excited state (blue circles) obtained for $(\text{CzBT})_2\text{-M}$. The 488 and 375 nm excitation correspond to the HOMO–LUMO transition and transition into the higher excited state.

spectrum of $(\text{CzBT})_2$ in a Zeonex film (Figure 10a, black line) was similar to that in a toluene solution (Figure 10a, dashed line). At the single-molecule level, the fluorescence spectra of $(\text{CzBT})_2$ molecules displayed peaks between 520 and 550 nm (Figure 10a colored lines). Spectral diffusion was not observed for the $(\text{CzBT})_2$ molecules. The peak positions and spectral widths obtained from individual $(\text{CzBT})_2$ molecules are plotted in Figure 10b (blue circles). The spectral widths of single molecules are narrower than that of the ensemble spectrum (Figure 10b, red line). The variations of the spectral peak position broaden the width of the ensemble spectrum. The distribution of the peak position could be interpreted either by slightly different local environments around each molecule⁴³ or slightly different twist angles in each molecule.

By contrast, a much broader distribution of the peak position was observed for the individual $(\text{CzBT})_n$ molecules embedded in the Zeonex film (Figure 10c (colored lines) and d (blue circles)). $(\text{CzBT})_n$ showed fluorescence peaks between 535 and 595 nm. Due to the broader peak distribution, an ensemble fluorescence spectrum of $(\text{CzBT})_n$ in the Zeonex film is much broader than that of the single molecules (Figure 10c (black line) and d (red line)).

While $(\text{CzBT})_2$ always showed constant fluorescence spectra, 27% (13/48) of the $(\text{CzBT})_n$ molecules showed clear spectral

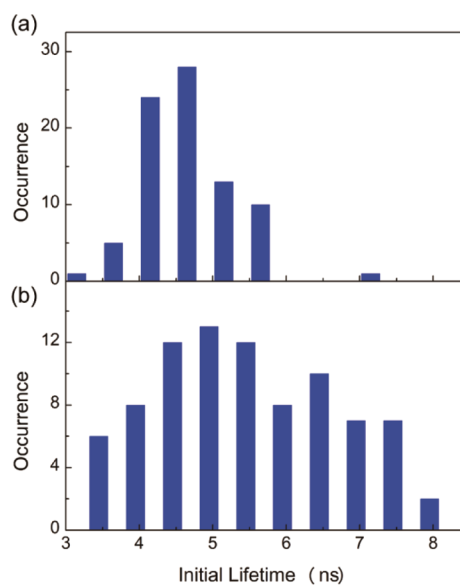


Figure 9. Frequency histograms of initial fluorescence lifetimes obtained from individual (a) $(\text{CzBT})_2$ and (b) $(\text{CzBT})_n$ molecules embedded in Zeonex thin films.

diffusion (Figure S16a). Spectral diffusion as large as up to 50 nm was observed. In most cases, spectral diffusion to the higher energy side occurred. Similar spectral shifts have been observed for other conjugated polymer molecules.^{29,87} This spectral change is a strong indication of the efficient exciton migration and trapping at the lowest energy units in individual $(\text{CzBT})_n$ molecules. The rest of the molecules did not display significant spectral diffusion (Figure S16b,c,d). The broad spectra observed in Figure S16b could be attributed to the presence of multiple energetically similar units within that the rapid exchanges of the emitting unit occur. Much narrower and constant spectra (Figure S16c,d) indicate the presence of only one emitting unit in the molecule.

The ensemble fluorescence spectrum of $(\text{CzBT})_n$ in the Zeonex film (Figure 10c, black line) displayed a large blue shift (25 nm) as compared with the ensemble spectrum measured in toluene (Figure 10c (broken line) and d (black line)). At the single-molecule level, the peak position of the spectra showed much large distribution compared with that of $(\text{CzBT})_2$ (Figure 10c (colored lines) and d (blue circles)). This result cannot be explained by heterogeneous microenvironments surrounding the molecules because $(\text{CzBT})_n$ displayed a smaller solvent-dependent spectral shift as compared with $(\text{CzBT})_2$ at the ensemble level (Figure 2d,f). The finding rather supports the twist structure of $(\text{CzBT})_n$ suggested by the single-molecule two-color excitation and lifetime experiments. Single-molecule spectra measurements of an annealed sample ($T_{\text{anneal}} = 438$ K) showed a broad distribution of the peak position (Figure S17), which suggested that complete structural relaxation of $(\text{CzBT})_n$ does not occur even in the sample annealed above the glass transition temperature of the host polymer Zeonex ($T_g = 411$ K). Some $(\text{CzBT})_n$ molecules showed red-shifted fluorescence spectra as compared with the $(\text{CzBT})_2$ molecules. The observed shifts could be attributed to intersegment interactions, such as aggregation.

Photophysical properties of conjugated polymers have been investigated within the context of intersegment interactions and whole-chain conformation. Especially at the single-molecule

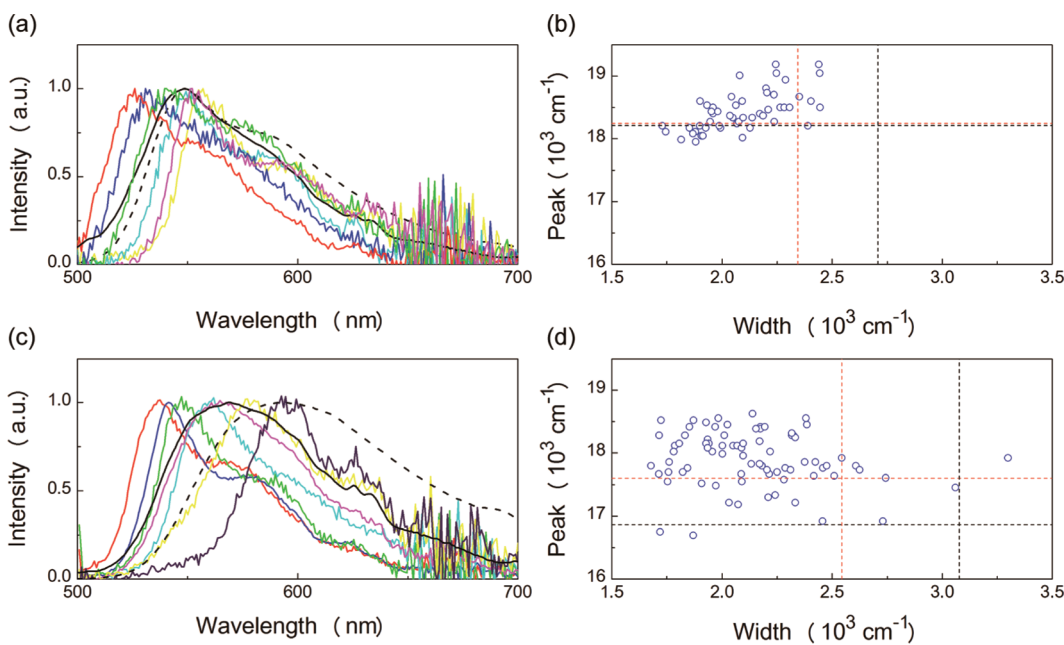


Figure 10. (a,c) Fluorescence spectra of single $(\text{CzBT})_2$ and $(\text{CzBT})_n$ molecules (colored lines) embedded in Zeonex thin films, respectively. Ensemble fluorescence spectra in toluene solution and Zeonex thin films are shown in dashed lines and black lines, respectively. (b,d) Correlation between the width and peak wavenumber of fluorescence spectra of individual $(\text{CzBT})_2$ and $(\text{CzBT})_n$ molecules, respectively. The black and red lines show the spectral widths and peak positions obtained from the ensemble spectra measured in toluene solution and Zeonex thin films, respectively.

level, most of the observed distributions of photophysical parameters have been connected mainly to the conformational diversity of the whole chain. Our findings suggest that this fundamental model has to be reviewed. We demonstrated clearly in this study that the intrasegment structures differ substantially among each molecule, and the structure is one of the crucial factors for the photophysical properties of the entire chains,^{37,39,78,89} at least in the case of D–A-type conjugated polymers.

Implications for Optoelectronic Applications. Our single-molecule experiments explicitly demonstrated that each $(\text{CzBT})_n$ molecule has distinct absorption and fluorescence spectra and fluorescence lifetime, depending of the twist angle. This would have significant effects on the optoelectronic applications.

Photovoltaic devices are one of the important potential applications of the D–A-type conjugated polymers. So far, great efforts have been made to achieve desired band gaps by fine-tuning chemical structures of each moiety.¹⁰ However, our results suggest that the chemical tuning of the band gap alone is not enough. For designing an efficient light harvesting system, physical control of the chain structure at the monomer unit level would also be critically important. In addition to the light harvesting property, charge separation efficiency is one of the critical parts for the photovoltaic devices. Exciton diffusion length is one of the controlling factors for the charge separation efficiency. The twist angle-dependent absorption and fluorescence spectra of $(\text{CzBT})_n$ imply the twist angle-dependent (Förster-type) exciton migration efficiency because the spectral overlap of the absorption and fluorescence is the major factor for the efficiency. Furthermore, the fluorescence lifetime, which is also related to the twist angle, would contribute to the exciton diffusion length since the diffusion occurs within the lifetime of the exciton. Actually, a recent theoretical study examined the possibility of regulating exciton migration length by controlling the excited state

lifetime.⁹⁰ These arguments indicate that the physical control of the structure at the monomer level also plays an essential role for regulating exciton diffusion process in conjugated polymers.

PLEDs, especially white light emitting devices are another important potential application of the D–A type conjugated polymers.⁹ Although we investigated the photoluminescence of $(\text{CzBT})_n$ in this study, not electroluminescence (EL), an EL spectrum should also be dependent on the twist structure. According to our experiments, the physical structure is directly related to the color of fluorescence. In order to obtain a desired color in an EL spectrum, a fine control of the physical structure would be necessary. Our results also indicate a potential possibility to actively tune and control the EL color by controlling the twist structure.

CONCLUSIONS

Excited-state dynamics in conjugated polymers plays a pivotal role in developing polymer-based optoelectronic devices. So far, intersegment interactions have been thought of as the primary factor for controlling exciton dynamics of conjugated polymers. In this study, by taking a combined approach of single-molecule fluorescence microscopy and DFT calculation, we investigated the spectroscopic properties of the D–A-type conjugated polymer $(\text{CzBT})_n$ in great detail, including absorption and fluorescence spectra, fluorescence lifetime, and intersegment exciton migration. We demonstrated that the intrasegment twist played a key role in deciding the spectroscopic characteristics of $(\text{CzBT})_n$. Our findings indicate that the intrasegment structures of conjugated polymers are one of the critical factors controlling exciton dynamics within the chain. Studies along this line will further bring about a better understanding of how intrasegment structures are related to the optical and electronic properties of conjugated polymers.

■ ASSOCIATED CONTENT

S Supporting Information. Details of syntheses, experimental procedures, DFT/TD-DFT calculation details, scheme of single-molecule experimental setups, absorption spectra in different solvents, ensemble fluorescence decay curves in solvents and in films, calculated Förster radius, calculated histograms of polarization value, data of single-molecule defocused imaging, single-molecule polarization imaging, and single-molecule spectra, single-molecule lifetime. This material is available free of charge via the Internet at <http://pubs.acs.org>.

■ AUTHOR INFORMATION

Corresponding Author

*Tel.: +81-3-5734-3643. Fax: +81-3-5734-2425. E-mail: habuchi.s.aa@m.titech.ac.jp.

■ ACKNOWLEDGMENT

The authors thank Dr. D. Das for her contribution in the initial stage of the study. This work was supported by Grant-in-Aid for Scientific Research No. 22750122 (S.H.) and No. 20340109 (M.V.) of the Japan Society for the Promotion of Science. S.H. is grateful for the Kurata Grant.

■ REFERENCES

- (1) Burroughes, J. H.; Bradley, D. D. C.; Brown, A. R.; Marks, R. N.; MacKay, K.; Friend, R. H.; Burns, P. L.; Holmes, A. B. *Nature* **1990**, *347*, 539–541.
- (2) Brabec, C. J.; Sariciftci, N. S.; Hummelen, J. C. *Adv. Funct. Mater.* **2001**, *11*, 15–26.
- (3) Dimitrakopoulos, C. D.; Malenfant, P. R. L. *Adv. Mater.* **2002**, *14*, 99–117.
- (4) Chen, L. H.; McBranch, D. W.; Wang, H. L.; Helgeson, R.; Wudl, F.; Whitten, D. G. *Proc. Natl. Acad. Sci. U.S.A.* **1999**, *96*, 12287–12292.
- (5) Thomas, S. W.; Joly, G. D.; Swager, T. M. *Chem. Rev.* **2007**, *107*, 1339–1386.
- (6) Wu, C.; Bull, B.; Szymanski, C.; Christensen, K.; McNeill, J. *ACS Nano* **2008**, *2*, 2415–2423.
- (7) Brabec, C. J.; Winder, C.; Sariciftci, N. S.; Hummelen, J. C.; Dhanabalan, A.; van Hal, P. A.; Janssen, R. A. J. *Adv. Funct. Mater.* **2002**, *12*, 709–712.
- (8) Soci, C.; Hwang, I. W.; Moses, D.; Zhu, Z.; Waller, D.; Gaudiana, R.; Brabec, C. J.; Heeger, A. J. *Adv. Funct. Mater.* **2007**, *17*, 632–636.
- (9) Jiang, J. X.; Xu, Y. H.; Yang, W.; Guan, R.; Liu, Z. Q.; Zhen, H. Y.; Cao, Y. *Adv. Mater.* **2006**, *18*, 1769–1773.
- (10) Muhlbacher, D.; Scharber, M.; Morana, M.; Zhu, Z. G.; Waller, D.; Gaudiana, R.; Brabec, C. J. *Adv. Mater.* **2006**, *18*, 2884–2889.
- (11) Schindler, F.; Jacob, J.; Grimsdale, A. C.; Scherf, U.; Mullen, K.; Lupton, J. M.; Feldmann, J. *Angew. Chem., Int. Ed.* **2005**, *44*, 1520–1525.
- (12) Gierschner, J.; Cornil, J.; Egelhaaf, H. J. *Adv. Mater.* **2007**, *19*, 173–191.
- (13) Klaerner, G.; Miller, R. D. *Macromolecules* **1998**, *31*, 2007–2009.
- (14) Padmanaban, G.; Ramakrishnan, S. *J. Am. Chem. Soc.* **2000**, *122*, 2244–2251.
- (15) Tsoi, W. C.; Charas, A.; Cadby, A. J.; Khalil, G.; Adawi, A. M.; Iraqi, A.; Hunt, B.; Morgado, J.; Lidzey, D. G. *Adv. Funct. Mater.* **2008**, *18*, 600–606.
- (16) Woo, H. S.; Lhost, O.; Graham, S. C.; Bradley, D. D. C.; Friend, R. H.; Quattrochi, C.; Bredas, J. L.; Schenk, R.; Mullen, K. *Synth. Met.* **1993**, *59*, 13–28.
- (17) Hennebicq, E.; Pourtois, G.; Scholes, G. D.; Herz, L. M.; Russell, D. M.; Silva, C.; Setayesh, S.; Grimsdale, A. C.; Mullen, K.; Bredas, J. L.; Beljonne, D. *J. Am. Chem. Soc.* **2005**, *127*, 4744–4762.
- (18) Ebihara, Y.; Habuchi, S.; Vacha, M. *Chem. Lett.* **2009**, *38*, 1094–1095.
- (19) Yu, J.; Hu, D. H.; Barbara, P. F. *Science* **2000**, *289*, 1327–1330.
- (20) Hollars, C. W.; Lane, S. M.; Huser, T. *Chem. Phys. Lett.* **2003**, *370*, 393–398.
- (21) Kumar, P.; Lee, T. H.; Mehta, A.; Sumpter, B. G.; Dickson, R. M.; Barnes, M. D. *J. Am. Chem. Soc.* **2004**, *126*, 3376–3377.
- (22) Barbara, P. F.; Gesquiere, A. J.; Park, S. J.; Lee, Y. J. *Acc. Chem. Res.* **2005**, *38*, 602–610.
- (23) Hu, D. H.; Yu, J.; Barbara, P. F. *J. Am. Chem. Soc.* **1999**, *121*, 6936–6937.
- (24) VandenBout, D. A.; Yip, W. T.; Hu, D. H.; Fu, D. K.; Swager, T. M.; Barbara, P. F. *Science* **1997**, *277*, 1074–1077.
- (25) Lammi, R. K.; Barbara, P. F. *Photochem. Photobiol. Sci.* **2005**, *4*, 95–99.
- (26) Laquai, F.; Park, Y. S.; Kim, J. J.; Basche, T. *Macromol. Rapid Commun.* **2009**, *30*, 1203–1231.
- (27) Scholes, G. D.; Rumbles, G. *Nat. Mater.* **2006**, *5*, 683–696.
- (28) Ebihara, Y.; Vacha, M. *J. Phys. Chem. B* **2008**, *112*, 12575–12578.
- (29) Huser, T.; Yan, M.; Rothberg, L. J. *Proc. Natl. Acad. Sci. U.S.A.* **2000**, *97*, 11187–11191.
- (30) Schwartz, B. J. *Annu. Rev. Phys. Chem.* **2003**, *54*, 141–172.
- (31) Sugimoto, T.; Habuchi, S.; Ogino, K.; Vacha, M. *J. Phys. Chem. B* **2009**, *113*, 12220–12226.
- (32) Vacha, M.; Habuchi, S. *NPG Asia Mater.* **2010**, *2*, 134–142.
- (33) Muls, B.; Uji-i, H.; Melnikov, S.; Moussa, A.; Verheijen, W.; Soumillion, J. P.; Josemon, J.; Mullen, K.; Hofkens, J. *ChemPhysChem* **2005**, *6*, 2286–2294.
- (34) Habuchi, S.; Onda, S.; Vacha, M. *Phys. Chem. Chem. Phys.* **2011**, *13*, 1743–1753.
- (35) Habuchi, S.; Onda, S.; Vacha, M. *Chem. Commun.* **2009**, 4868–4870.
- (36) Bolinger, J. C.; Traub, M. C.; Adachi, T.; Barbara, P. F. *Science* **2011**, *331*, 565–567.
- (37) Donley, C. L.; Zaumseil, J.; Andreasen, J. W.; Nielsen, M. M.; Sirringhaus, H.; Friend, R. H.; Kim, J. S. *J. Am. Chem. Soc.* **2005**, *127*, 12890–12899.
- (38) Lupton, J. M. *Adv. Mater.* **2010**, *22*, 1689–1721.
- (39) Becker, K.; Da Como, E.; Feldmann, J.; Scheliga, F.; Csanyi, E. T.; Tretiak, S.; Lupton, J. M. *J. Phys. Chem. B* **2008**, *112*, 4859–4864.
- (40) Letard, J. F.; Lapouyade, R.; Rettig, W. *J. Am. Chem. Soc.* **1993**, *115*, 2441–2447.
- (41) Fron, E.; Deres, A.; Rocha, S.; Zhou, G.; Mullen, K.; De Schryver, F. C.; Sliwa, M.; Uji-i, H.; Hofkens, J.; Vosch, T. *J. Phys. Chem. B* **2010**, *114*, 1277–1286.
- (42) Cotlet, M.; Masuo, S.; Luo, G. B.; Hofkens, J.; Van der Auweraer, M.; Verhoeven, J.; Mullen, K.; Xie, X. L. S.; De Schryver, F. *Proc. Natl. Acad. Sci. U.S.A.* **2004**, *101*, 14343–14348.
- (43) Izquierdo, M. A.; Bell, T. D. M.; Habuchi, S.; Fron, E.; Pilot, R.; Vosch, T.; De Feyter, S.; Verhoeven, J.; Jacob, J.; Mullen, K.; Hofkens, J.; De Schryver, F. C. *Chem. Phys. Lett.* **2005**, *401*, 503–508.
- (44) Morin, J. F.; Leclerc, M.; Ades, D.; Siove, A. *Macromol. Rapid Commun.* **2005**, *26*, 761–778.
- (45) Blouin, N.; Leclerc, M. *Acc. Chem. Res.* **2008**, *41*, 1110–1119.
- (46) Li, J. L.; Dierschke, F.; Wu, J. S.; Grimsdale, A. C.; Mullen, K. *J. Mater. Chem.* **2006**, *16*, 96–100.
- (47) Li, J. L.; Grimsdale, A. C. *Chem. Soc. Rev.* **2010**, *39*, 2399–2410.
- (48) Michinobu, T.; Osako, H.; Shigehara, K. *Macromolecules* **2009**, *42*, 8172–8180.
- (49) Michinobu, T.; Osako, H.; Murata, K.; Shigehara, K. *Chem. Lett.* **2010**, *39*, 168–169.
- (50) Michinobu, T.; Osako, H.; Shigehara, K. *Macromol. Rapid Commun.* **2008**, *29*, 111–116.
- (51) Cotlet, M.; Hofkens, J.; Maus, M.; Gensch, T.; Van der Auweraer, M.; Michiels, J.; Dirix, G.; Van Guyse, M.; Vanderleyden, J.; Visser, A.; De Schryver, F. C. *J. Phys. Chem. B* **2001**, *105*, 4999–5006.
- (52) Habuchi, S.; Cotlet, M.; Hofkens, J.; Dirix, G.; Michiels, J.; Vanderleyden, J.; Subramaniam, V.; De Schryver, F. C. *Biophys. J.* **2002**, *83*, 3499–3506.

- (53) Habuchi, S.; Satoh, N.; Yamamoto, T.; Tezuka, Y.; Vacha, M. *Angew. Chem., Int. Ed.* **2010**, *49*, 1418–1421.
- (54) Habuchi, S.; Oba, T.; Vacha, M. *Phys. Chem. Chem. Phys.* **2011**, *13*, 6970–6976.
- (55) Habuchi, S.; Tsutsui, H.; Kochaniak, A. B.; Miyawaki, A.; van Oijen, A. M. *PLoS One* **2008**, *3*, e3944.
- (56) Cotlet, M.; Hofkens, J.; Habuchi, S.; Dirix, G.; Van Guyse, M.; Michiels, J.; Vanderleyden, J.; De Schryver, F. C. *Proc. Natl. Acad. Sci. U.S.A.* **2001**, *98*, 14398–14403.
- (57) Habuchi, S.; Ando, R.; Dedecker, P.; Verheijen, W.; Mizuno, H.; Miyawaki, A.; Hofkens, J. *Proc. Natl. Acad. Sci. U.S.A.* **2005**, *102*, 9511–9516.
- (58) Frisch, M. J. et al. *Gaussian 09*; Gaussian, Inc.: Wallingford CT, 2009.
- (59) Parr, R. G.; Yang, W. *Density-Functional Theory of Atoms and Molecules in Chemistry*; Springer-Verlag: New York, 1991.
- (60) Yanai, T.; Tew, D. P.; Handy, N. C. *Chem. Phys. Lett.* **2004**, *393*, 51–57.
- (61) Jacquemin, D.; Perpete, E. A.; Scuseria, G. E.; Ciofini, I.; Adamo, C. *J. Chem. Theory Comput.* **2008**, *4*, 123–135.
- (62) Curutchet, C.; Feist, F. A.; Van Averbekke, B.; Mennucci, B.; Jacob, J.; Mullen, K.; Basche, T.; Beljonne, D. *Phys. Chem. Chem. Phys.* **2010**, *12*, 7378–7385.
- (63) Casida, M. E. *Recent Advances in Density Functional Methods*; World Scientific: Singapore, 1995.
- (64) Huang, J.; Niu, Y. H.; Yang, W.; Mo, Y. Q.; Yuan, M.; Cao, Y. *Macromolecules* **2002**, *35*, 6080–6082.
- (65) Michinobu, T.; Okoshi, K.; Sako, H.; Kumazawa, H.; Shigehara, K. *Polymer* **2008**, *49*, 192–199.
- (66) Ambrose, J. F.; Carpenter, L. L.; Nelson, R. F. *J. Electrochem. Soc.* **1975**, *122*, 876–894.
- (67) Shen, M.; Rodriguez-Lopez, J.; Huang, J.; Liu, Q. A.; Zhu, X. H.; Bard, A. J. *J. Am. Chem. Soc.* **2010**, *132*, 13453–13461.
- (68) Henry, B. R.; Morrison, J. D. *J. Mol. Spectrosc.* **1975**, *55*, 311–318.
- (69) Maus, M.; Rettig, W.; Bonafoux, D.; Lapouyade, R. *J. Phys. Chem. A* **1999**, *103*, 3388–3401.
- (70) Anemian, R.; Mulatier, J. C.; Andraud, C.; Stephan, O.; Vial, J. C. *C. Chem. Commun.* **2002**, 1608–1609.
- (71) Chi, C. Y.; Im, C.; Wegner, G. *J. Chem. Phys.* **2006**, *124*, 024907.
- (72) Hsu, J. H.; Fann, W. S.; Tsao, P. H.; Chuang, K. R.; Chen, S. A. *J. Phys. Chem. A* **1999**, *103*, 2375–2380.
- (73) Jakubiak, R.; Collison, C. J.; Wan, W. C.; Rothberg, L. J.; Hsieh, B. R. *J. Phys. Chem. A* **1999**, *103*, 2394–2398.
- (74) Smilowitz, L.; Hays, A.; Heeger, A. J.; Wang, G.; Bowers, J. E. *J. Chem. Phys.* **1993**, *98*, 6504–6509.
- (75) Cornil, J.; Gueli, I.; Dkhissi, A.; Sancho-Garcia, J. C.; Hennebicq, E.; Calbert, J. P.; Lemaur, V.; Beljonne, D.; Bredas, J. L. *J. Chem. Phys.* **2003**, *118*, 6615–6623.
- (76) Winfield, J. M.; Van Vooren, A.; Park, M. J.; Hwang, D. H.; Cornil, J.; Kim, J. S.; Friend, R. H. *J. Chem. Phys.* **2009**, *131*, 035104.
- (77) Piacenza, M.; Comoretto, D.; Burger, M.; Morandi, V.; Marabelli, F.; Martinelli, C.; Farinola, G. M.; Cardone, A.; Gigli, G.; Della Sala, F. *ChemPhysChem* **2009**, *10*, 1284–1290.
- (78) Schmidtke, J. P.; Kim, J. S.; Gierschner, J.; Silva, C.; Friend, R. H. *Phys. Rev. Lett.* **2007**, *99*, 167401.
- (79) Bohmer, M.; Enderlein, J. *J. Opt. Soc. Am. B* **2003**, *20*, 554–559.
- (80) Uji-i, H.; Melnikov, S. M.; Deres, A.; Bergamini, G.; De Schryver, F.; Herrmann, A.; Mullen, K.; Enderlein, J.; Hofkens, J. *Polymer* **2006**, *47*, 2511–2518.
- (81) Dedecker, P.; Muls, B.; Deres, A.; Uji-i, H.; Hotta, J.; Sliwa, M.; Soumillion, J. P.; Mullen, K.; Enderlein, J.; Hofkens, J. *Adv. Mater.* **2009**, *21*, 1079–1090.
- (82) Sugimoto, T.; Ebihara, Y.; Ogino, K.; Vacha, M. *ChemPhysChem* **2007**, *8*, 1623–1628.
- (83) Fron, E.; Bell, T. D. M.; Van Vooren, A.; Schweitzer, G.; Cornil, J.; Beljonne, D.; Toeple, P.; Jacob, J.; Mullen, K.; Hofkens, J.; Van der Auweraer, M.; De Schryver, F. C. *J. Am. Chem. Soc.* **2007**, *129*, 610–619.
- (84) Flors, C.; Oesterling, I.; Schnitzler, T.; Fron, E.; Schweitzer, G.; Sliwa, M.; Herrmann, A.; van der Auweraer, M.; de Schryver, F. C.; Mullen, K.; Hofkens, J. *J. Phys. Chem. C* **2007**, *111*, 4861–4870.
- (85) Vosch, T.; Fron, E.; Hotta, J.; Deres, A.; Uji-i, H.; Idrissi, A.; Yang, J.; Kim, D.; Puhl, L.; Haeseler, A.; Mullen, K.; De Schryver, F. C.; Sliwa, M.; Hofkens, J. *J. Phys. Chem. C* **2009**, *113*, 11773–11782.
- (86) Melnikov, S. M.; Yeow, E. K. L.; Uji-i, H.; Cotlet, M.; Mullen, K.; De Schryver, F. C.; Enderlein, J.; Hofkens, J. *J. Phys. Chem. B* **2007**, *111*, 708–719.
- (87) Sartori, S. S.; De Feyter, S.; Hofkens, J.; Van der Auweraer, M.; De Schryver, F.; Brunner, K.; Hofstraat, J. W. *Macromolecules* **2003**, *36*, 500–507.
- (88) Yan, M.; Rothberg, L. J.; Papadimitrakopoulos, F.; Galvin, M. E.; Miller, T. M. *Phys. Rev. Lett.* **1994**, *73*, 744–747.
- (89) Khalil, G. E.; Adawi, A. M.; Fox, A. M.; Iraqi, A.; Lidzey, D. G. *J. Chem. Phys.* **2009**, *130*, 044903.
- (90) Van Averbekke, B.; Beljonne, D. *ChemPhysChem* **2009**, *10*, 3061–3068.